

In-gas-cell laser spectroscopy for magnetic dipole moment of ^{199}Pt toward $N = 126$

Y. Hirayama,^{1,*} M. Mukai,^{2,1,3} Y.X. Watanabe,¹ S.C. Jeong,^{4,1} H.S. Jung,¹ Y. Kakiguchi,¹
S. Kimura,^{2,1,3} J.Y. Moon,⁴ M. Oyaizu,¹ J.H. Park,⁴ P. Schury,¹ M. Wada,^{1,3} and H. Miyatake¹

¹*Wako Nuclear Science Center (WNSC), Institute of Particle and Nuclear Studies (IPNS),
High Energy Accelerator Research Organization (KEK), Wako, Saitama 351-0198, Japan*

²*University of Tsukuba, Tsukuba, Ibaraki 305-0006, Japan*

³*Nishina Center for Accelerator-Based Science, RIKEN, Wako, Saitama 351-0198, Japan*

⁴*Rare Isotope Science Project, Institute for Basic Science (IBS), Daejeon 305-811, Republic of Korea*

(Dated: March 19, 2018)

Magnetic dipole moment and mean-square charge radius of ^{199}Pt ($I^\pi = 5/2^-$) have been evaluated for the first time from the investigation of the hyperfine splitting of the $\lambda_1 = 248.792$ nm transition by in-gas-cell laser ionization spectroscopy. Neutron-rich nucleus ^{199}Pt was produced by multi-nucleon transfer reaction at the KISS where the nuclear spectroscopy in the vicinity of $N = 126$ is planned from the aspect of an astrophysical interest as well as the nuclear structure. Measured magnetic dipole moment $+0.63(13)\mu_N$ is consistent with the systematics of those of nuclei with $I^\pi = 5/2^-$. The deformation parameter $|\langle \beta_2^2 \rangle^{1/2}|$ evaluated from the isotope shift indicates the gradual shape change to spherical shape of platinum isotopes with increasing neutron number toward $N = 126$.

I. INTRODUCTION

Allowed Gamow-Teller (GT) and first-forbidden (FF) beta-decay transitions compete in the nuclei around $N = 126$, depending on the shell evolution at increasing the number of neutrons. The proton orbit of the neutron-rich nuclei around $N = 126$ would be $\pi(0h_{11/2})$, therefore, the GT transition from $\nu(0h_{9/2})$ to $\pi(0h_{11/2})$, and the FF transition from $\nu(0i_{13/2})$ to $\pi(0h_{11/2})$ would be competitive. This makes it difficult to predict nuclear properties such as the half-life and nuclear mass in the neutron-rich nuclei around $N = 126$ by theoretical nuclear models [1–3]. Therefore, the half-lives are largely deviated by one order of magnitude [4–8]. The half-lives play an important role to investigate an astrophysical environment for the formation of the third peak in an observed solar r-process abundance pattern [9, 10]. Because the abundance peak height around $A = 195$ is proportional to the half-lives, and the peak position and width drastically change according to the half-lives. The experimental nuclear spectroscopy are desirable for eliminating the uncertainty and improving the predictions by nuclear models taking into account the FF transition.

The study of nuclear structure toward $N = 126$ through electromagnetic moments has been intensively performed by various techniques suitable for the nuclear properties such as half-life, level energy and decay modes [11]. The nuclear wave-function and shape can be evaluated from the measured magnetic dipole moment (μ) and quadrupole moment (Q), respectively. Especially, the understanding of the wave function on the ground state in this region is essential to provide the accurate prediction of GT and FF transition strength, namely, β -decaying half-lives. However, the difficulty of the pro-

duction of the nuclei in the vicinity of $N = 126$ causes the lack of the electromagnetic moments. In order to break through the situation, we have started KISS project [12]. In the project, the nuclei around $N = 126$ are produced by multi-nucleon transfer (MNT) reaction [13] of ^{136}Xe beam and ^{198}Pt target system [14], and are selected by an argon gas-cell based laser ion source combined with on-line isotope separator (KISS) [15, 16]. The electromagnetic moments can be measured by in-gas-cell and -gas-jet laser ionization spectroscopy (IGLIS) [17–19].

By taking the advantage of the MNT reaction combined with the KISS, we have started to produce the neutron-rich isotopes of the refractory elements such as Pt, Ir, Os, Re, W and Ta, and perform the nuclear spectroscopy systematically. The search for the laser resonance ionization scheme of the refractory elements has been in progress [20–22]. As a first step, the measurement of the magnetic dipole moment of ^{199}Pt ($Z = 78$, $N = 121$, $I^\pi = 5/2^-$, and $t_{1/2} = 30.8(2)$ min.) [23] was performed by in-gas-cell laser ionization spectroscopy. Nuclear structure of platinum isotopes with $178 \leq A \leq 198$ have been well studied through the measured μ and Q , isotope shift (IS) and charge radius by the laser spectroscopy [24–28]. In the lighter, neutron-deficient, region of $178 \leq A \leq 183$, shape coexistence was found and discussed from the IS [28]. On the other hand, in the heavier region of $183 \leq A \leq 198$, the prolate ($183 \leq A \leq 188$), triaxial shape ($190 \leq A \leq 194$) and oblate ($196 \leq A \leq 198$) shapes were discussed and compared with theoretical models [24–27]. In the more neutron-rich region, spherical shape would become dominant toward the shell-closure of $N = 126$ in the same way as lead ($Z = 82$) and mercury ($Z = 80$) isotopes [29] predicted by the droplet model [30] with $\beta_2 = 0$. In this paper, we report the experimental details and the results for the in-gas-cell laser ionization spectroscopy to determine the magnetic dipole moment of neutron-rich ^{199}Pt .

* yoshikazu.hirayama@kek.jp

II. EXPERIMENT

A. Principle of laser spectroscopy for deducing nuclear electromagnetic moments

Laser spectroscopy is a powerful tool to determine nuclear electromagnetic moments through the investigation of hyperfine levels governed by quantum number F . The possible F values are in the range of $|I - J| \leq F \leq I + J$ where I and J are nuclear and atomic spins, respectively. According to F values, if $I > 1/2$, the degenerated atomic energy levels are resolved and changed by ΔE which is denoted as following;

$$\Delta E = \frac{A}{2} \times K + \frac{B}{2} \times \frac{3K(K+1) - 2I(I+1)2J(J+1)}{2I(2I-1)2J(2J-1)}, \quad (1)$$

$$K = F(F+1) - I(I+1) - J(J+1).$$

Here, A and B are the magnetic-dipole and electric-quadrupole hyperfine coupling constants, respectively. These factors are represented to be

$$A = \frac{\mu H_{JJ}(0)}{IJ} \quad (2)$$

and

$$B = eQ\phi_{JJ}(0) \quad (I, J > 1/2), \quad (3)$$

respectively. The A and B factors are related to the nuclear magnetic dipole moment μ and nuclear electric quadrupole moment Q , respectively. $H_{JJ}(0)$ and $\phi_{JJ}(0)$ are the magnetic field and the electric field gradient, respectively, induced by the atomic electrons at the position of the nucleus. $H_{JJ}(0)$ and $\phi_{JJ}(0)$ are specific to each atomic state, and are common for isotopes. Therefore, nuclear electromagnetic moments can be evaluated from the measured A and B factors by using the known A' and B' factors, I' , μ' , and Q' of specific isotope (generally stable isotope) as follows;

$$\mu = \frac{I}{I'} \frac{A}{A'} \mu', \quad (4)$$

and

$$Q = \frac{B}{B'} Q' \quad (I, J > 1/2). \quad (5)$$

The atomic energy changes of ΔE_{gs} and ΔE_{ex} at the ground and excited states occur, respectively, as a result of hyperfine interaction between the nucleus and atomic electrons. The transition frequency between the hyperfine levels of the ground and excited states shifts to be

$$\Delta\nu_i = \Delta E_{i,\text{ex}} - \Delta E_{i,\text{gs}} \quad (6)$$

relative to the center of gravity of the fine-structure transition-frequency ν_0 . From the laser spectroscopy for the measurement of the hyperfine splitting expressed by the $\Delta\nu_i$ values, the hyperfine coupling constants A and B , namely, electromagnetic moments μ and Q , can be evaluated.

B. Experimental details

1. KISS

The experiment was performed using KEK isotope separation system (KISS) [15, 16], argon gas-cell based laser ion source combined with on-line isotope separator, installed in RIKEN Nishina center. Primary beam ^{136}Xe (10.75 MeV/A, 20 particle-nA), accelerated by RIKEN Ring Cyclotron, impinged on an enriched ^{198}Pt (purity 91.63%) target with a thickness of 11 mg/cm². Unstable nucleus ^{199}Pt was produced by multi-nucleon transfer reaction [14], and stable nucleus ^{198}Pt was also emitted from the target by an elastic reaction with ^{136}Xe . At an off-line test to study the systematics of the laser ionization for platinum isotopes, the stable platinum isotopes of $^{192,194,195,196,198}\text{Pt}$ were produced from the resistive heating of a natural platinum filament placed in the gas cell.

The platinum isotopes were accumulated, thermalized and neutralized in the argon gas cell with a pressure of 88 kPa, whose design was optimized for the high efficient gas-flow transport [15]. The isotopes were re-ionized in the gas cell by two-step resonant laser ionization technique, and the atomic number Z can be selected. The laser-produced singly-charged ($q = 1$) platinum ions were extracted with an energy of 20 kV, and their mass-to-charge ratio (A/q) was selected by a dipole magnet. Finally, one kind of isotope was transported to the detector station placed at the neighboring experimental hall to the gas cell system.

The detector station includes a tape transport device for avoiding the radioactivities in the decay chain of separated nuclides under pulsed beam operation of the KISS. The radioactive isotope was implanted on an aluminized Mylar tape surrounded by three sets of two-layered plastic-scintillator telescopes with 50% detection efficiency [31]. The tape was moved to remove unwanted β -rays at the end of each measurement cycle. The ions of the stable isotopes were counted by using a Channeltron detector.

2. Laser ionization

Figure 1 shows the ionization scheme and hyperfine structure of platinum isotopes. Tunable dye laser (Radiant Dye Laser; NarrowScan) pumped by XeCl:excimer laser ($\lambda = 308$ nm, Lambda Physik LPX240i) was utilized for the first step excitation ($\lambda_1 = 248.792$ nm) with laser

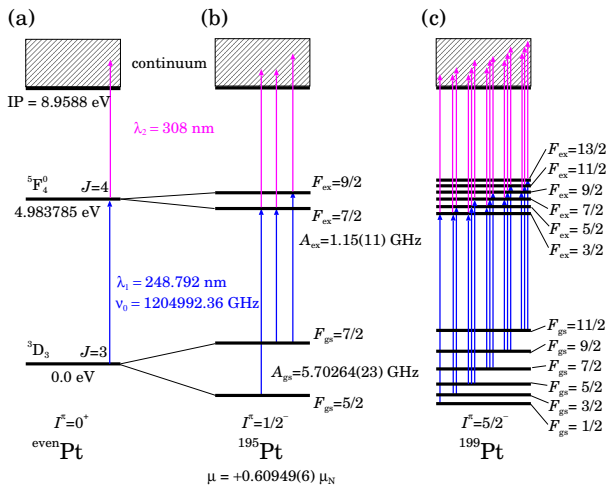


FIG. 1. Ionization scheme and hyperfine structure of platinum isotopes. (a) in the case of $^{\text{even}}\text{Pt}$ with $I^\pi = 0^+$, there is no hyperfine splitting. (b) in the case of ^{195}Pt with $I^\pi = 1/2^-$ and $\mu = +0.60949(6) \mu_N$, the hyperfine splitting is governed by only A_{gs} and A_{ex} factors, and there are three transitions. (c) in the case of ^{199}Pt with $I^\pi = 5/2^-$, the hyperfine splitting of $F_{\text{gs}} = 1/2-11/2$ and $F_{\text{ex}} = 3/2-13/2$ is governed by A and B factors of the ground and excited states, and there are 15 transitions.

power $70 \mu\text{J}/\text{pulse}$. Another XeCl excimer laser of $\lambda_2 = 308 \text{ nm}$ with laser power $9 \text{ mJ}/\text{pulse}$ was used as the ionization transition to continuum above the ionization potential (IP). In the present laser ionization spectroscopy, the transition between the ground state $5d^96s^3D_3$ and the excited state $5d^86s6p^5F_4^0$ was studied by scanning the wavelength λ_1 . The systematic study concerning the gas-pressure effects was performed by using stable platinum isotopes with mass number $A = 192, 194, 195, 196$, and 198 . Pressure broadening and shift in the range of $11-88 \text{ kPa}$ were studied to be $39(3) \text{ MHz}/\text{kPa}$ and $-22(2) \text{ MHz}/\text{kPa}$, respectively. Isotope shifts for the stable platinum isotopes were also studied.

The excimer lasers were operated at a repetition rate of up to 200 Hz and were synchronized by master trigger signals from a function generator. To produce a UV laser beam as first step light, radiation delivered by the NarrowScan was frequency doubled using a barium borate (BBO) crystal placed in a second-harmonic generator. The typical linewidth and pulse width of the dye lasers were 3.4 GHz and 15 ns , and the wavelength was monitored by a wave-meter WS6 (HighFinesse). The 10% of UV laser power through a laser beam splitter was monitored during the experiment. The distance between the laser system and the gas cell is about 15 m . Both laser beams with the size of about $8-10 \text{ mm}$ in diameter are transported to the gas cell with a small angle, and are overlapped in the gas cell for resonance ionization, spatially and temporally. The laser spots through the gas cell was checked by using a camera in order to keep the

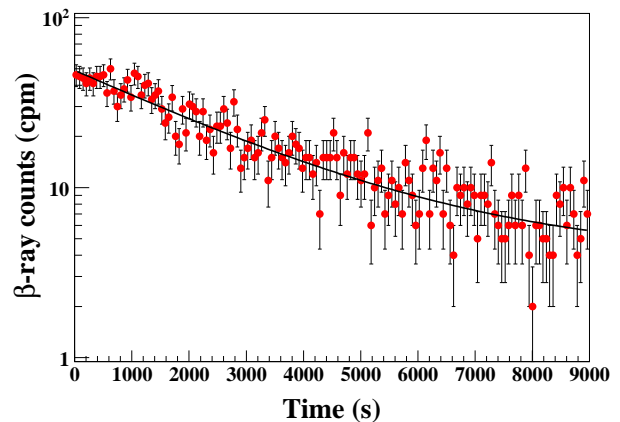


FIG. 2. Measured decay curve of ^{199}Pt nucleus, which was used for the identification of the ^{199}Pt nucleus extracted from the KISS.

spatial overlap by adjusting the mirrors with actuators. The timing signals from photodetectors were measured by an oscilloscope in order to maintain temporal overlap of the two lasers by adjusting the master trigger signal in 1-ns steps. The spatial and temporal overlapping were always monitored and adjusted if necessary.

III. EXPERIMENTAL RESULTS AND DISCUSSION

A. Identification of ^{199}Pt nucleus

In the experiment, the laser-ionized $^{198}\text{Pt}^+$ was used to adjust the beam line optics at first. Then, the extraction of laser-ionized radioactive isotope $^{199}\text{Pt}^+$ was performed only by changing the magnetic field of the dipole magnet. Identification of $^{199}\text{Pt}^+$ nucleus ($t_{1/2} = 30.8 \pm 0.2 \text{ min}$. [23]) was done by measuring the β -decay half-life $t_{1/2}$ as shown in Fig. 2. After 30 min . irradiation of $^{199}\text{Pt}^+$ beam on the tape, the decay curve was measured during 2.5 hours ($\approx 5 \times t_{1/2}$). Solid line in Fig. 2 is the best fit result obtained by using the fitting routine of MINUIT code [32], and the fitting function consists of single exponential function (free parameters of amplitude and $t_{1/2}$) and constant background. Measured half-life $t_{1/2} = 31.3 \pm 1.5 \text{ min}$. was in good agreement with the literature value $t_{1/2} = 30.8(2) \text{ min}$. This result indicates that measured β -rays were emitted from only $^{199}\text{Pt}^+$ extracted from the gas cell.

B. Extraction yield of ^{199}Pt nucleus

In the present experiment, the relative extracted yield of ^{199}Pt nucleus was measured as a function of wavelength of λ_1 , and the hyperfine splitting was studied to

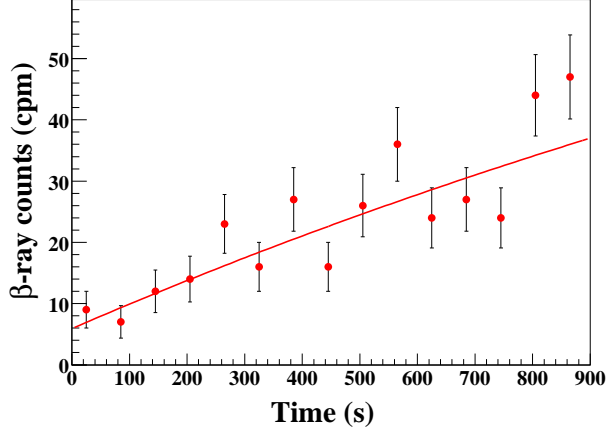


FIG. 3. Typical growth curve of ^{199}Pt nucleus, which was measured for the evaluation of relative extraction yield I_0 of ^{199}Pt nucleus extracted from the KISS.

evaluate the magnetic dipole moment. Relative extraction yield I_0 was deduced from the growth curve during 15 min. irradiation as shown in Fig. 3. Solid line in Fig. 3 is the best fit result, and the fitting function consists of single exponential function (free parameter of amplitude I_0) and constant background. The fluctuations of the primary beam intensity, laser powers, wavelength λ_1 within 0.2 pm, spacial and temporal overlapping influenced the number of measured β -rays emitted from ^{199}Pt nucleus. The growth curve in Fig. 3 reflected the fluctuations, and, therefore, the evaluated I_0 and its error δI_0 take the fluctuations into account automatically. The I_0 and δI_0 were normalized by the measured primary beam dose during each measurement.

C. Data analysis of hyperfine splitting

Figure 4 shows the measured hyperfine splittings of $^{198,195,199}\text{Pt}$ nuclei extracted from the KISS. The line shape of a resonance peak was determined from the fit of the measured single peak of ^{198}Pt ($I^\pi = 0^+$) as shown in Fig. 4-(a). The A_{ex} factor for the excited state $5d^86s6p^5F_4^0$ was deduced for the first time from the spectrum analysis of ^{195}Pt ($I^\pi = 1/2^-$ and $\mu = +0.60949(6) \mu_N$ [26]) in Fig. 4-(b). In order to determine magnetic dipole moment μ and IS $\delta\nu$, the deduced line shape and A_{ex} factor were applied for the spectrum analysis of ^{199}Pt ($I^\pi = 5/2^-$) in Fig. 4-(c). The details of the analysis are discussed at the following subsections.

1. Line shape

There is no hyperfine splitting for ^{198}Pt with $I^\pi = 0^+$ as shown in Fig. 1-(a), and, therefore, a single resonance peak was observed as shown in Fig. 4-(a). The line

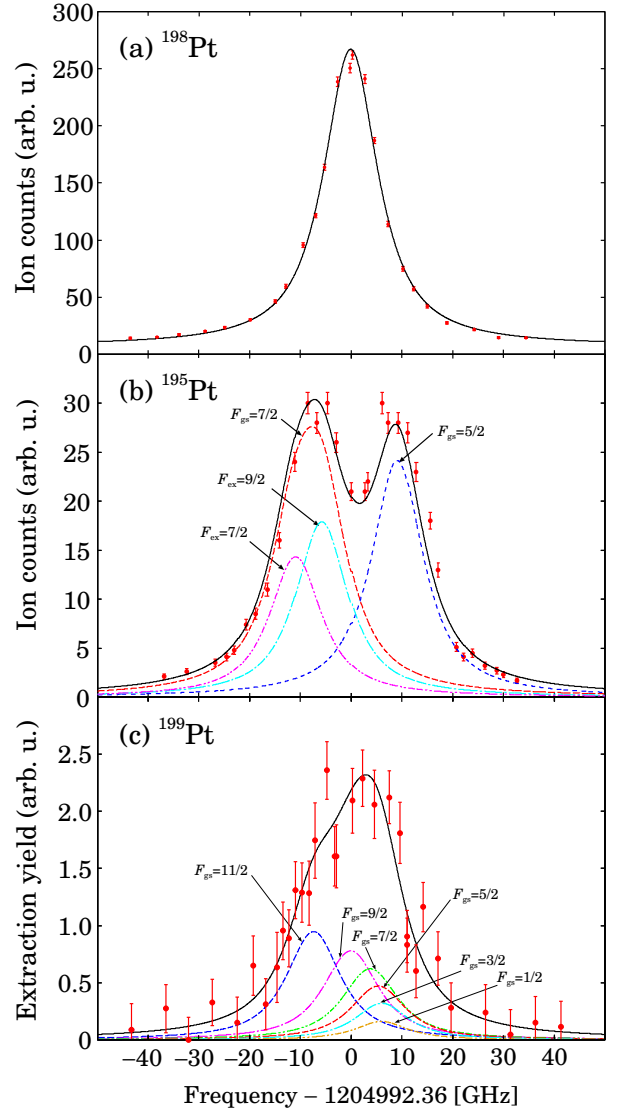


FIG. 4. Measured hyperfine splittings of $^{198,195,199}\text{Pt}$ nuclei extracted from the KISS. The experimental conditions of gas pressure and laser power of λ_1 were 88 kPa and 70 $\mu\text{J}/\text{pulse}$, respectively. (a) the analysis of the single resonance peak of ^{198}Pt nucleus provides the line shape measured under the experimental conditions. (b) in the spectrum of ^{195}Pt nucleus, the line shapes labeled as $F_{\text{gs}} = 5/2$ and $7/2$ indicate the transitions from both the levels to the excited states. The line shapes labeled as $F_{\text{ex}} = 7/2$ and $9/2$ indicate the components of the transitions from $F_{\text{gs}} = 7/2$ to each excited hyperfine-level. (c) in the spectrum of ^{199}Pt nucleus, the line shapes labeled as $F_{\text{gs}} = 1/2, 3/2, 5/2, 7/2, 9/2,$ and $11/2$ indicate the transitions from each hyperfine-level on the ground state to the excited states as shown in Fig. 1-(c), and consist of the transitions from the each level to the excited hyperfine-levels in the same manner as the transitions of ^{195}Pt isotope.

shape is Voigt function which is composed of the convolution of Gaussian and Lorentzian components. The line shape, as shown in Fig. 4–(a), is governed mainly by Lorentzian components in the present experiment. The two Gaussian components are Doppler broadening governed by the argon gas temperature and laser linewidth, whose width in FWHM were evaluated to be 1.0 GHz at 300 K and 3.4 GHz, respectively. As a result, total Gaussian width of 3.5 GHz was obtained and used as a fixed parameter in all fits. Lorentzian components consist of gas-pressure broadening, laser-power broadening, and the natural width 63 MHz of the present transition. The width of Lorentzian components was free parameter in the fitting, and was deduced to be 11.8(4) GHz. As a result, total FWHM 12.8(4) GHz was obtained. The measured line shape of ^{198}Pt at the on-line experiment was applied to other isotopes as the fixed parameter for the fitting of the spectra. All fits in the present analysis were performed by using the MINUIT code [32].

2. Hyperfine coupling constant A_{ex}

The hyperfine splitting of ^{195}Pt with $I^\pi = 1/2^-$ and $\mu = +0.60949(6) \mu_{\text{N}}$ [23] is governed by A_{gs} and A_{ex} factors, and there are three transitions as shown in Fig. 1–(b). A_{gs} was precisely measured to be 5.70264(23) GHz [33]. However, A_{ex} of the excited level was unknown. The fit to the measured spectrum of ^{195}Pt in Fig. 4–(b) is able to provide the A_{ex} factor. The line shape of the three transitions are unity, and each resonance peak position presented by Eq. (6) depends on the A_{ex} factor (here, $B_{\text{gs}} = B_{\text{ex}} = 0$), which was free as the fitting parameter.

Another important parameter is an amplitude of each resonance peak. In order to reduce the fitting parameters and constrain the amplitude, the relative intensity [34] for each transition was applied in the present analysis. The relative intensities of the transitions from the $F_{\text{gs}} = 5/2$ and $7/2$ levels are in proportion to the statistical weights $(2F_{\text{gs}} + 1)$, and are assumed to be 6/14 and 8/14, respectively. In the present experiment, both $F_{\text{ex}} = 7/2$ and $9/2$ levels would be populated by two transitions from $F_{\text{gs}} = 7/2$ simultaneously due to the broad line shape. The relative intensities for the transitions $F_{\text{gs}} = 7/2 \rightarrow F_{\text{ex}} = 7/2$ and $9/2$ are also in proportion to the statistical weights $(2F_{\text{ex}} + 1)$, and are estimated to be 8/18 and 10/18, respectively. Finally, the relative intensities for the three transitions of $F_{\text{gs}} = 5/2 \rightarrow F_{\text{ex}} = 7/2$, $F_{\text{gs}} = 7/2 \rightarrow F_{\text{ex}} = 7/2$, and $F_{\text{gs}} = 7/2 \rightarrow F_{\text{ex}} = 9/2$ are constrained to be 6/14, 8/14 \times 8/18, and 8/14 \times 10/18, respectively, and one fitting parameter for the amplitude was used.

The solid black line indicates the best fit to the spectrum in Fig. 4, taking into account the isotope shift as the fixed parameter. The IS value was evaluated from the measured ones by using $^{192,194,196,198}\text{Pt}$ isotopes, considering the linear relation of the isotope shift [25, 26]. The $A_{\text{ex}} = 1.15 \pm 0.11$ GHz was obtained as a best fit re-

sult. Even though the experimental conditions such as gas pressure and laser power of λ_1 were different, the deduced A_{ex} factor was consistent with each other. The A_{ex} factor was used for the spectrum analysis of ^{199}Pt isotope.

3. Magnetic dipole moment of ^{199}Pt

Fig. 4–(c) shows the measured hyperfine structure of ^{199}Pt . Relative extraction yields as mentioned in Sec. IIIB were measured as a function of λ_1 . In order to confirm the consistency of the yield I_0 during the long-run measurement, the three-times frequency-scanning in the range $-40 \leq \Delta\nu_0 \leq +40$ GHz were performed. Finally, the consistency of the measured yield I_0 was confirmed.

The hyperfine splitting of $F_{\text{gs}} = 1/2-11/2$ and $F_{\text{ex}} = 3/2-13/2$ for ^{199}Pt with $I = 5/2$ is governed by A and B factors of the ground and excited states, and there are 15 transitions as shown in Fig. 1. Each resonance peak position presented by Eq. (6) depends on unknown μ , Q , B_{ex} factor, and $\Delta\nu_0$ (shift from the center of the gravity $\nu_0 = 1204992.36$ GHz), which were free as the fitting parameters. Here, the B_{gs} factor of the ground state is related to the Q by $B_{\text{gs}} = -Q/0.685$ GHz from Ref. [26], and this equation was used in the fitting. The line shape for each transition was fixed to that evaluated from ^{198}Pt , and the relative intensities of the 15 transitions were constrained by using the statistical weights of $(2F_{\text{gs}} + 1)$ and $(2F_{\text{ex}} + 1)$ in the same manner as the fitting procedure of ^{195}Pt .

The solid black line indicates the best fit to the spectrum in Fig. 4. Measured μ , Q and B_{ex} were $0.63 \pm 0.13(\text{stat.}) \pm 0.03(\text{syst.}) \mu_{\text{N}}$, -2.7 ± 3.0 b, -1.8 ± 9.4 GHz, respectively. Here, the fitting errors were corrected by the square root of reduced χ^2 1.14 of the fitting. The systematic error stems from the ambiguity of the width of the line shape and A_{ex} . The width of the spectrum is mainly governed by the magnetic dipole moment of ^{199}Pt nucleus. Therefore, it was possible to deduce the μ value. The Q and B_{ex} were insensitive to the spectrum fitting. Even though the Q and B_{ex} were artificially assumed to be 0, this affects the deviation $\Delta\mu = 0.015 \mu_{\text{N}}$ which is negligible in considering the present error.

Table. I shows the systematics of magnetic dipole moments of nuclei with $I^\pi = 5/2^-$. $I^\pi = 5/2^-$ is determined by one valence neutron in $2f_{5/2}$ orbit, whose Schmidt value is evaluated to $+1.366 \mu_{\text{N}}$. Although the present $\mu = 0.63(13)$ is smaller than the systematics of about $+0.85$ for the nuclei, it is consistent with the systematics by taking the error into account. The μ values in Table. I is about 60% of Schmidt value. This indicates that large configuration mixing exists in the wave-function of these states.

TABLE I. Systematics of magnetic dipole moments of nuclei with $I^\pi = 5/2^-$.

Nuclide	I^π	$t_{1/2}$	E_x (keV)	μ (μ_N)	Q (b)	Method	Ref.
$^{199}_{78}\text{Pt}$	$5/2^-$	30.8(2) min.	0	$+0.63 \pm 0.13(\text{stat.}) \pm 0.03(\text{syst.})$	-2.7 ± 3.0	IGLIS	Present work
$^{195}_{78}\text{Pt}$	$5/2^-$	0.67(3) ns	130	+0.875(100)	-	Mössbauer	[35]
$^{197}_{78}\text{Pt}$	$5/2^-$	16.58(17) ns	53.088	+0.85(3)	-	TDPAC	[36]
$^{197}_{80}\text{Hg}$	$5/2^-$	8.066(8) ns	134	+0.855(15)	-0.081(6)	TDPAC	[37]
$^{199}_{80}\text{Hg}$	$5/2^-$	2.45(5) ns	158	+0.880(33)	+0.95(7)	TDPAC	[37]

4. Isotope shift and deformation parameter of ^{199}Pt

Measured isotope shift (IS) between ^{198}Pt and ^{199}Pt was $\delta\nu^{198,199} = 0.98 \pm 0.48$ GHz. Table II shows the summary of the measured isotope shifts of the wavelength $\lambda_1 = 248.792$ nm, isotopic variation of the mean-square charge radius from Ref. [26], and quadrupole deformation parameters calculated by using the droplet model [30]. The IS $\delta\nu^{A,A'} = \nu_0^{A'} - \nu_0^A$ between two isotopes with mass number A and A' is expressed as

$$\delta\nu^{A,A'} = (K_{\text{NMS}} + K_{\text{SMS}}) \times \frac{m_{A'} - m_A}{m_{A'} m_A} + F_{248} \times \delta < r^2 >^{A,A'}. \quad (7)$$

Here, K_{NMS} and K_{SMS} are factors for normal (NMS) and specific (SMS) mass shift components, respectively. The term $F_{248} \times \delta < r^2 >^{A,A'}$ is the field shift (FS) component expressed by using the electronic factor F_{248} for the transition $\lambda_1 = 248.792$ nm and the isotopic variation of the mean-square charge radius $\delta < r^2 >^{A,A'}$.

In order to deduce $\delta < r^2 >^{A,A'}$ from measured $\delta\nu^{A,A'}$, the Eq. (7) can be practically modified as follows;

$$\delta < r^2 >^{A,A'} \frac{m_{A'} m_A}{m_{A'} - m_A} = -\frac{K_{\text{MS}}}{F_{248}} + \frac{1}{F_{248}} \delta\nu^{A,A'} \frac{m_{A'} m_A}{m_{A'} - m_A} \quad (8)$$

Here, $K_{\text{MS}} = K_{\text{FMS}} + K_{\text{SMS}}$. If both $\delta\nu^{A,A'}$ and $\delta < r^2 >^{A,A'}$ for stable isotopes were known, K_{MS} and F_{248} can be evaluated for deducing the $\delta < r^2 >^{A,A'}$ from measured $\delta\nu^{A,A'}$. Generally, the term of the mass shift (\sim a few 10 MHz) is about two order of magnitude smaller than the term of the field shift (\sim a few GHz) in the present high $Z = 78$ region [38], and the mass shift term can be negligible in the present case. The factor F_{248} was evaluated to 17.0 ± 1.8 GHz/fm² from the fit using Eq. (8) between the measured $\delta\nu^{A,A'}$ and the reported $\delta < r^2 >^{A,A'}$ [26] for ^{even}Pt in Table II. Finally, the $\delta < r^2 >^{198,199} = 0.057(29)$ fm² ($\delta < r^2 >^{194,199} = 0.208(30)$) was obtained from the $\delta\nu^{198,199} = 0.98(48)$ GHz. Figure 5 shows the mean square charge radius variation of the platinum isotopes [26, 28]. The evaluated $\delta < r^2 >^{194,199}$ shows the linear relation of platinum isotopes with $193 \leq A \leq 198$.

Model-dependent quadrupole deformation parameter $< \beta_2^2 >$ can be extracted from the measured $\delta\nu^{A,A'}$ and

TABLE II. Measured isotope shifts $\delta\nu_{\text{exp}}^{194,A}$ and $\delta\nu_{\text{exp}}^{198,199}$, isotopic variation of the mean-square charge radius $\delta < r^2 >^{194,199}$ and $\delta < r^2 >^{194,A}$ from Ref. [26]. Quadrupole deformation parameters $\delta < \beta >^{194,A}$ and $< \beta_2^2 >^{1/2}$ calculated by using Droplet model [30].

A	$\delta\nu_{\text{exp}}^{194,A}$ [GHz]	$\delta < r^2 >^{194,A}$ [fm ²]	$\delta < \beta >^{194,A}$	$ < \beta_2^2 >^{1/2} $
199	0.98(48) ^a	0.208(30) ^b	-0.067(10) ^b	0.115(10) ^b
198	2.43(23) ^b	0.151(6)	-0.0050(7)	0.12(1)
196	1.39(27) ^b	0.074(4)	-0.0027(3)	0.13(1)
194	0.000	0.000	0.000	0.1434(26)
192	-1.43(27) ^b	-0.072(3)	0.0033(9)	0.15(1)

^a Present work : measured isotope shift $\delta\nu_{\text{exp}}^{198,199}$.

^b Present work

$\delta < r^2 >^{A,A'}$. The details of the extraction procedure and the utilization for the platinum isotopes were reported in Ref. [39] and Ref. [26], respectively. The evaluated parameters $\delta < \beta_2^2 >$ and $| < \beta_2^2 >^{1/2} |$ were listed in Table II. The absolute deformation parameter $| < \beta_2^2 >^{1/2} |$ for ^{199}Pt was evaluated from the relation of $< \beta_2^2 >^A = < \beta_2^2 >^{194} + \delta < \beta_2^2 >^{194,A}$. Here, the parameter $< \beta_2^2 >^{194}$ was deduced by using the precisely measured $B(E2, 2^+ \rightarrow 0^+)$ value of ^{194}Pt [40], and the evaluated parameters $< \beta_2^2 >^{\text{evenPt}}$ were in good agreement with the known $B(E2)$ values [40] for ^{even}Pt. The evaluated $\delta < \beta_2^2 >$ also shows the linear relation of platinum isotopes with $193 \leq A \leq 198$. The $| < \beta_2^2 >^{1/2} |$ for ^{199}Pt becomes smaller with increasing neutron number toward $N = 126$ as shown in Fig. 5, indicating the spherical shape for platinum isotope with $N = 126$.

IV. SUMMARY

Neutron-rich nucleus ^{199}Pt ($I^\pi = 5/2^-$) was produced by multi-nucleon transfer reaction at the KISS, where the nuclear spectroscopy around $N = 126$ have been performed from the aspect of an astrophysical interest as well as the nuclear structure. Magnetic dipole moments provide the crucial information about the nuclear wave-function, which is essential for the understanding of the competition between allowed Gamow-Teller (GT) and first-forbidden (FF) beta-decay transitions in the nuclei around $N = 126$.

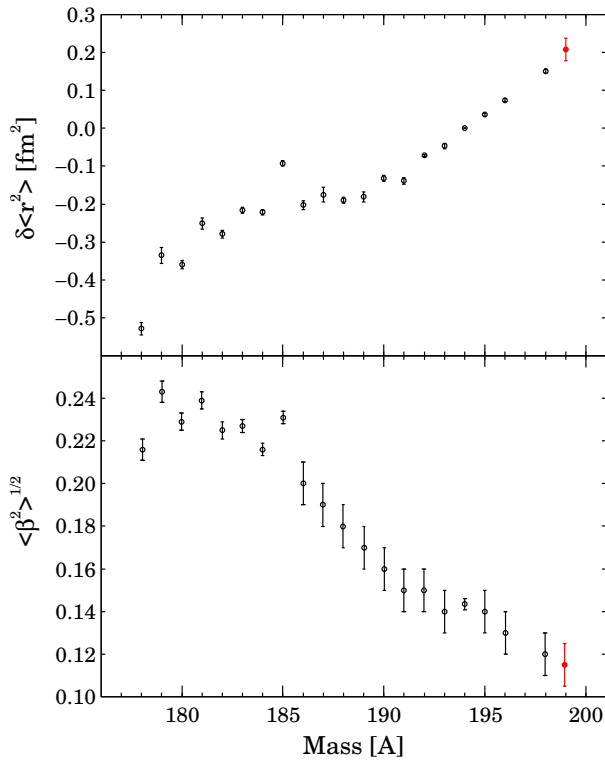


FIG. 5. Systematics of mean square charge radius variation $\delta \langle r^2 \rangle^{194,A}$ and quadrupole deformation parameter $|\langle \beta_2^2 \rangle^{1/2}|$ as a function of mass number A of the platinum isotopes. Open and closed circles present the values from Ref. [26, 28] and by the present work, respectively.

By in-gas-cell laser ionization spectroscopy performed at the KISS, magnetic dipole moment μ and mean-square charge radius variation $\delta \langle r^2 \rangle^{194,199}$ of ^{199}Pt have been determined for the first time to be $+0.63(13) \mu_N$ and $0.208(30) \text{ fm}^2$. Measured magnetic dipole moment is consistent with the systematics of those of nuclei with $I^\pi = 5/2^-$. The evaluated parameters $\delta \langle \beta_2^2 \rangle$ and $|\langle \beta_2^2 \rangle^{1/2}|$ were consistent with the linear relation of platinum isotopes with $193 \leq A \leq 198$. The behavior with increasing neutron number toward $N = 126$ would indicate the shape change to spherical shape of platinum isotopes.

By taking the advantage of the MNT reaction combined with the KISS, systematical nuclear spectroscopy is planned for the neutron-rich isotopes of the refractory elements such as Pt, Ir, Os, Re, W and Ta.

ACKNOWLEDGMENTS

This experiment was performed at RI Beam Factory operated by RIKEN Nishina Center and CNS, the University of Tokyo. The authors acknowledge the staff of the accelerator for their support. This work has been supported by Grant-in-Aids for Scientific Research (A) (grant no. 23244060, 26247044 and 15H02096) and for young scientists (B) (grant no. 24740180) from the Japan Society for the Promotion of Science (JSPS).

-
- [1] I. N. Borzov, *Phys. Rev. C* **67**, 025802 (2003).
[2] P. Möller, B. Pfeiffer, and K.-L. Kratz, *Phys. Rev. C* **67**, 055802 (2003).
[3] H. Koura, T. Tachibana, M. Uno, and M. Yamada, *Prog. Theor. Phys.* **113**, 305 (2005).
[4] P. Möller, J. R. Nix, and K.-L. Kratz, *At. Data Nucl. Data Tables* **66**, 131 (1997).
[5] J. Engel, M. Bender, J. Dobaczewski, W. Nazarewicz, and R. Surman, *Phys. Rev. C* **60**, 014302 (1999).
[6] G. Martinez-Pinedo, *Nucl. Phys. A* **688**, 357c (2001).
[7] K. Langanke and G. Martinez-Pinedo, *Rev. Mod. Phys.* **75**, 819 (2003).
[8] KUTY, <http://wwwndc.jaea.go.jp/nucldata/beta-decay-properties.pdf>.
[9] E. M. Burbidge, G. R. Burbidge, W. A. Fowler, and F. Hoyle, *Rev. Mod. Phys.* **29**, 547 (1957).
[10] M. R. Mumpower, R. Surman, G. C. McLaughlin, and A. Aprahamian, *Prog. Part. Nucl. Phys.* **86**, 86 (2016).
[11] N. J. Stone, *Table of Nuclear Magnetic Dipole and Electric Quadrupole Moments* (2011).
[12] S. C. Jeong, N. Imai, H. Ishiyama, Y. Hirayama, H. Miyatake, and Y. X. Watanabe, KEK Report **2010-2** (2010).
[13] C. H. Dasso, G. Pollarolo, and A. Winther, *Phys. Rev. Lett.* **73**, 1907 (1994).
[14] Y. X. Watanabe, Y. H. Kim, S. C. Jeong, Y. Hirayama, N. Imai, H. Ishiyama, H. S. Jung, H. Miyatake, S. Choi, J. S. Song, E. Clement, G. de France, A. Navin, M. Rejmund, C. Schmitt, G. Pollarolo, L. Corradi, E. Fioretto, D. Montanari, M. Niikura, D. Suzuki, H. Nishibata, and J. Takatsu, *Phys. Rev. Lett.* **115**, 172503 (2015).
[15] Y. Hirayama, Y. X. Watanabe, N. Imai, H. Ishiyama, S. C. Jeong, H. Miyatake, M. Oyaizu, S. Kimura, M. Mukai, Y. H. Kim, T. Sonoda, M. Wada, M. Huyse, Y. Kudryavtsev, and P. V. Duppen, *Nucl. Instrum. Methods Phys. Res. B* **353**, 4 (2015).
[16] Y. Hirayama, Y. X. Watanabe, N. Imai, H. Ishiyama, S. C. Jeong, H. S. Jung, H. Miyatake, M. Oyaizu, S. Kimura, M. Mukai, Y. H. Kim, T. Sonoda, M. Wada, M. Huyse, Y. Kudryavtsev, and P. V. Duppen, *Nucl. Instrum. Methods Phys. Res. B* **376**, 52 (2016).
[17] T. E. Cocolios, A. N. Andreyev, B. Bastin, N. Bree, J. Büscher, J. Elseviers, J. Gentens, M. Huyse, Y. Kudryavtsev, D. Pauwels, T. Sonoda, P. V. den Bergh, and P. V. Duppen, *Phys. Rev. C* **81**, 014314 (2010).
[18] R. Ferrer, N. Bree, T. E. Cocolios, I. G. Darby, H. D. Witte, W. Dexters, J. Diriken, J. Elseviers, S. Franchoo, M. Huyse, N. Kesteloot, Y. Kudryavtsev, D. Pauwels, D. Radulov, T. Roger, H. Savajols, P. V. Duppen, and M. Venhart, *Phys. Lett. B* **728**, 191 (2014).
[19] Y. Kudryavtsev, R. Ferrer, M. Huyse, P. V. den Bergh,

- and P. V. Duppen, Nucl. Instrum. Methods Phys. Res. B **297**, 7 (2013).
- [20] Y. Hirayama, M. Mukai, Y. X. Watanabe, N. Imai, H. Ishiyama, S. C. Jeong, H. Miyatake, M. Oyaizu, Y. Matsuo, T. Sonoda, and M. Wada, J. Phys. B **47**, 075201 (2014).
- [21] M. Mukai, Y. Hirayama, N. Imai, H. Ishiyama, S. C. Jeong, H. Miyatake, M. Oyaizu, Y. X. Watanabe, Y. H. Kim, and S. Kimura, JPS. Conf. Proc. **6**, 030127 (2015).
- [22] M. Mukai, Y. Hirayama, H. Ishiyama, H. S. Jung, H. Miyatake, M. Oyaizu, Y. X. Watanabe, S. Kimura, A. Ozawa, S. C. Jeong, and T. Sonoda, Nucl. Instrum. Methods Phys. Res. B **376**, 73 (2016).
- [23] R. B. Firestone, *Table of Isotopes* (John Wiley & Sons, Inc., 1996).
- [24] J. K. P. Lee, G. Savard, J. E. Crawford, G. Thekkadath, H. T. Duong, J. Pinard, S. Liberman, F. L. Blanc, P. Kilcher, J. Obert, J. Oms, J. C. Putaux, B. Roussi re, and J. Sauvage, Phys. Rev. C **38**, 2985 (1988).
- [25] H. T. Duong, J. Pinard, S. Liberman, G. Savard, J. K. P. Lee, J. E. Crawford, G. Thekkadath, F. L. Blanc, P. Kilcher, J. Obert, J. Oms, J. C. Putaux, B. Roussi re, J. Sauvage, and the ISOCELE Collaboration, Phys. Lett. B **217**, 401 (1989).
- [26] T. Hilberath, S. Becker, G. Bollen, H.-J. Kluge, U. Kr nert, G. Passler, J. Rikovska, R. Wyss, and the ISOLDE Collaboration, Z. Phys. A – Hadrons and Nuclei **342**, 1 (1992).
- [27] P. Kilcher, J. C. Putaux, J. E. Crawford, H. Dautet, H. T. Duong, F. L. Blanc, J. K. P. Lee, J. Obert, J. Oms, J. Pinard, B. Roussi re, J. Sauvage, G. Savard, and G. Thekkadath, Nucl. Instrum. Methods Phys. Res. B **70**, 537 (1992).
- [28] F. L. Blanc, D. Lunney, J. Obert, J. Oms, J. C. Putaux, B. Roussi re, J. Sauvage, S. Zemlyanoi, J. Pinard, L. Cabaret, H. T. Duong, G. Huber, M. Krieg, V. Sebastian, M. G. adn S. P ru, and J. Genevey, Phys. Rev. C **60**, 054310 (1999).
- [29] H. D. Witte1, A. N. Andreyev, N. Barr , M. Bender, T. E. Cocolios, S. Dean, D. Fedorov, V. N. Fedoseyev, L. M. Fraile, S. Franchoo, V. Hellemans, P. H. Heenen, K. Heyde, G. Huber, M. Huuse, H. Jeppessen, U. K ster, P. Kunz, S. R. Leshner, B. A. Marsh, I. Mukha, B. Roussi re, J. Sauvage, M. Seliverstov, I. Stefanescu, E. Tengborn, K. V. de Vell, J. V. de Walle, P. V. Duppen, and Y. Volkov, Phys. Rev. Lett. **98**, 112502 (2007).
- [30] W. D. Myers and K.-H. Schmidt, Nucl. Phys. A **410**, 61 (1983).
- [31] S. Kimura, H. Ishiyama, H. Miyatake, Y. Hirayama, Y. X. Watanabe, H. S. Jung, M. Oyaizu, M. Mukai, S. C. Jeong, and A. Ozawa, Nucl. Instrum. Methods Phys. Res. B **376**, 338 (2016).
- [32] CERN Program Library entry D506.
- [33] S. B ttgenbach, N. Glaeser, B. Roski, and R. Tr ber, Z. Phys. A – Atoms and Nuclei **317**, 237 (1984).
- [34] U. K ster, N. J. Stone, K. T. Flanagan, J. R. Stone, V. N. Fedosseev, K. L. Kratz, B. A. Marsh, T. Materna, L. Mathieu, P. L. Mokkanov, M. D. Seliverstov, O. Serot, A. M. Sj din, and Y. M. Volkov, Phys. Rev. C **84**, 034320 (2011).
- [35] B. Wolbeck and K. Zioutas, Nucl. Phys. A **181**, 289 (1972).
- [36] R. N. Saxena and J. C. Soares, Hyperfine Interact. **9**, 93 (1981).
- [37] K. Krien, K. Kroth, H. Saitovitch, and W. Thomas, Z. Phys. A **283**, 337 (1977).
- [38] K. Blaum, J. Dilling, and W. N rtersh user, Phys. Scr. T **152**, 014017 (2013).
- [39] S. Ahmad, W. Klempt, C. Ekstr m, R. Neugart, K. Wendt, and the ISOLDE collaboration, Z. Phys. A – Atoms and Nuclei **321**, 35 (1985).
- [40] S. Raman, J. Nestor, S. Kahane, and K. Bhatt, At. Data Nucl. Data Tables **42**, 1 (1989).